THE JOURNAL OF PHYSICAL CHEMISTRY A

Subscriber access provided by UNIV OF CALIFORNIA SAN DIEGO LIBRARIES

Article

Structural Analysis of Perfluoropropanoyl Fluoride in the Gas, Liquid and Solid Phases

Yanina Berrueta Martínez, Christian G. Reuter, Yury V. Vishnevskiy, Yanina
Belén Bava, Andrea Lorena Picone, Rosana Mariel Romano, Hans-Georg
Stammler, Beate Neumann, Norbert W. Mitzel, and Carlos Omar Della Védova

J. Phys. Chem. A, **Just Accepted Manuscript** • DOI: 10.1021/acs.jpca.6b00424 • Publication Date (Web): 29 Mar 2016

Downloaded from http://pubs.acs.org on March 31, 2016

Just Accepted

"Just Accepted" manuscripts have been peer-reviewed and accepted for publication. They are posted online prior to technical editing, formatting for publication and author proofing. The American Chemical Society provides "Just Accepted" as a free service to the research community to expedite the dissemination of scientific material as soon as possible after acceptance. "Just Accepted" manuscripts appear in full in PDF format accompanied by an HTML abstract. "Just Accepted" manuscripts have been fully peer reviewed, but should not be considered the official version of record. They are accessible to all readers and citable by the Digital Object Identifier (DOI®). "Just Accepted" is an optional service offered to authors. Therefore, the "Just Accepted" Web site may not include all articles that will be published in the journal. After a manuscript is technically edited and formatted, it will be removed from the "Just Accepted" Web site and published as an ASAP article. Note that technical editing may introduce minor changes to the manuscript text and/or graphics which could affect content, and all legal disclaimers and ethical guidelines that apply to the journal pertain. ACS cannot be held responsible for errors or consequences arising from the use of information contained in these "Just Accepted" manuscripts.

ACS Publications

The Journal of Physical Chemistry A is published by the American Chemical Society.
1155 Sixteenth Street N.W., Washington, DC 20036

Published by American Chemical Society. Copyright © American Chemical Society.
However, no copyright claim is made to original U.S. Government works, or works
produced by employees of any Commonwealth realm Crown government in the course
of their duties.

Structural Analysis of Perfluoropropanoyl Fluoride in the Gas, Liquid and Solid Phases

Yanina Berrueta Martínez, [†] *Christian G. Reuter,* [⊥] *Yury V. Vishnevskiy,* [⊥] *Yanina B. Bava,* [†] *Lorena A. Picone,* [†] *Rosana M. Romano,* [†] *Hans-Georg Stammler,* [⊥] *Beate Neumann,* [⊥] *Norbert W. Mitzel,* [⊥] *and Carlos O. Della Védova* [†,*]

†CEQUINOR (UNLP-CONICET), Departamento de Química, Facultad de Ciencias Exactas, Universidad Nacional de La Plata,
47 esq. 115, 1900 La Plata, República Argentina.

⊥Lehrstuhl für Anorganische Chemie und Strukturchemie, Centre for Molecular Materials CM$_2$, Bielefeld University,
Universitätsstraße 25, 33615 Bielefeld, Germany.

[*] *carlosdv@quimica.unlp.edu.ar*

ABSTRACT

The coexistence of two conformers in perfluoropropanoyl fluoride, $CF_3CF_2C(O)F$, with the CC−CF dihedral angle (*gauche* 85(10) % and *anti* 15(10) %) has been determined by means of gas phase electron diffraction (GED). Quantum-chemical calculations performed at the MP2 and B3LYP approximations and cc-pVTZ basis sets reproduce the experimental values with confidence. By contrast, FTIR spectra give no clear evidence for the *anti*-conformer in the gas phase. Information on this less abundant but stable rotamer was obtained from matrix-isolation/FTIR spectroscopy and liquid Raman spectroscopy. *In situ* crystallization and single crystal X-ray diffraction (XRD) data reveal the presence of solely the *gauche*-conformation in the solid state. A set of intermolecular interactions including C=O···C=O, C–F···F–C and F···C=O were detected. The nature of bonding and the relative stabilities of *gauche*- and *anti*-conformers were explored using natural bond orbitals.

KEY WORDS: Gas electron diffraction, X-ray diffraction, perfluoropropanoyl fluoride, gas infrared spectrum, hydrolysis, matrix isolation, liquid Raman spectrum.

INTRODUCTION

A wide variety of scientific and technological applications require perfluorinated compounds due to their singular and particular characteristics. Their high chemical and biological stability is conferred by the nature of the carbon-fluorine bond. Thus, applications are related to their properties as water and grease repelling coatings, standing textiles, adhesives, batteries, fuel cells, agrochemicals, and pharmaceutical products. This long list which includes different areas confirms the strengths and versatility of these compounds.[1,2] On the other hand, their release to the environment and the subsequently implied pollution transformed their study and use into a global concern issue.[3] Some of these compounds were dangerously found in human blood and many of them are spread all over the world due to their chemical persistence.[4] They have been identified in Antartic as well as in Artic regions.

Perfluoropronanoyl fluoride (PFPF), $CF_3CF_2C(O)F$, contains a short perfluorinated alkyl-chain and a concomitant high vapor pressure. For this reason it has also been found in the atmosphere,[5] and consequently is there a demand for a detailed knowledge of these species being the title molecule a good candidate. The high vapor pressure of the compound invites studying it in the gas phase by spectroscopic and diffraction techniques. On the other side, the crystal structure of PFPF can reveal information on the diversity of intermolecular interactions, which are of importance for crystal engineering and predominantly in the production of different drugs.[6] Here we offer a detailed characterization of this model molecule.

EXPERIMENTAL SECTION AND THEORETICAL METHODS

Synthesis

PFPF was synthesized by heating perfluoropropanoyl chloride with sodium fluoride in the presence of acetonitrile for 2 h at 70°C. In agreement with Vilenchik et al.[7] an almost quantitative yield was achieved. In an alternative method a mixture of $SbCl_5$ (0.15 ml), SbF_3 (3 g) and $CF_3CF_2C(O)Cl$ (2.0 ml) in sulfolane (6.0 ml) as solvent was reacted at 100º C. In this case only 50 % yield was attained. $CF_3CF_2C(O)F$ is very difficult to separate from the $CF_3CF_2C(O)Cl$ precursor since both have high vapor pressure and small amounts of the starting materials are always found in the products. In conclusion, the method reported by Vilenchik[7] is simpler and more efficient in terms of purity and yield.

Quantum-chemical calculations

The Gaussian 03 program[8] was used to perform quantum-chemical calculations, among with the calculation of the potential energy function about a specific dihedral angle is included, followed by the geometry optimization of the corresponding minima and the calculation of their harmonic frequencies. For these purposes B3LYP[9] and MP2[10] methods were chosen in conjunction with the cc-pVTZ basis set.[11] NBO[12] calculations were run with the NBO 5.G package[13] incorporated in Gaussian 03. The dimeric structure was also computed using Gaussian 03. In this case a potential energy curve and the corresponding optimization of the minimum obtained were performed with the B3LYP/6-311+G(d) level of approximation.

Analytical harmonic and the numeric cubic force fields for the gas electron diffraction (GED) analysis have been computed with the B3LYP/cc-pVTZ approximation. Using these data mean-square interatomic vibrational amplitudes and vibrational corrections to the equilibrium structure were calculated with the SHRINK program.[14,15,16]

Infrared spectra

Infrared spectra (IR) were recorded with a Nicolet™ 6700 spectrometer using a double wall cell with 100 mm optical path length and Si windows of 0.5 mm thickness. The resolution and the number of scans were 0.5 cm^{-1} and 64, respectively.

Matrix isolation

The gas mixture was deposited on a 15 K CsI window using the pulse deposition technique.[17,18,19] The low temperature was achieved by means of a Displex closed-cycle refrigerator (SHI-APD Cryogenics, model DE-202). The corresponding FTIR spectra were acquired using the instrument described earlier. A Spectra-Physics Hg-Xe arc lamp operating at 1000 W was used to irradiate the matrix in the 200 – 800 nm broad range. In order to avoid the matrix heating, a water filter was place between the lamp and the matrix. Several spectra were recorded at different irradiation time.

Annealing experiments were performed by warming up to 25 K and then freezing down to the original temperature of the matrix.

Raman spectra

The dispersive Raman spectra of the liquid were obtained by means of a Horiba-Jobin-Yvon T64000 Raman spectrometer, with a confocal microscope and CCD detection. A 514.5 nm excitation laser was used (Ar). The calibration was performed with the 459 cm^{-1} band of CCl_4.

UV/Vis spectra

A double beam UV−2600 Shimazdu spectrometer with a Lo-Ray-Light grade blazed holographic grating monochromator and a R-928 photomultiplier detector were used to record the UV/Vis spectra. The PFPF gas phase UV/Vis spectrum was recorded between 800 and 185 nm with 0.01 nm resolution.

X−Ray diffraction

A single crystal of PFPF was grown in situ in a capillary. This was achieved by first establishing a solid-liquid equilibrium close to the melting point at 146 K, then melting all solid but a tiny crystal seed (using a thin copper wire as external heat source) followed by slowly lowering the temperature until the whole capillary was filled with a single crystalline specimen and afterward chilling to 100K with 44 K per hour. The crystal was kept at 100.0(1) K during data collection on a Agilent SuperNova diffractometer at Bielefeld University. Using Olex2,[20] the structure was solved by direct methods and refined using the SHELX-97 [21] package.

Gas electron diffraction

The Balzers Eldigraph KD−G2 gas-phase electron diffractometer[22] at Bielefeld University was used to measure diffraction patterns on Fuji BAS MP 2025 imaging plates. The plates have been scanned on a calibrated Fuji BAS-1800II scanner. Table S1 (S denotes material in the Supporting Information) describes the experimental set up. After scanning the imaging plates, intensity curves (Figures S1 and S2) were obtained according to the method described by Vishnevskiy.[23] In the same experiments diffraction patterns of benzene have been measured and used for calibration of the sector function and electron wavelengths as usually.[24] For refinements in UNEX v1.6b program[25] molecular geometries were defined in form of Z-matrices and the independent geometrical parameters were refined in groups (see Tables S2 – S3). Differences between parameters in groups have been taken from MP2/cc-pVTZ calculations and were kept fixed during refinements. Experimental amplitudes were also refined in groups (Tables S4 – S5), keeping ratios between different amplitudes in each group constant at the theoretical values. In the refinement of the title compound, only one GED model corresponding to the mixture of both (*gauche* and *anti,* with respect to the CC-CF dihedral angle, respectively) conformers was used. This model described experimental data very well (R_f = 4.65 %, which is close to the estimated experimental error) and the refined parameters were physically sound and consistent. Therefore, there was no need to use a dynamic model in the present study. All correlations between refined parameters were below 0.7.

RESULTS AND DISCUSSION

Computational calculations

Conformational study of the monomer

In order to find out which conformations are expected to coexist in equilibrium in the gas phase at room temperature, the potential energy function about the dihedral angle Φ(CC−CF) of perfluoropropanoyl fluoride (PFPF), $CF_3CF_2C(O)F$, has been calculated using the approximations B3LYP/cc-pVTZ and MP2/cc-pVTZ (Figure 1). The scan calculated with the B3LYP level computes a lower energy barrier than the MP2,[26] however, both methods exhibit very similar results.

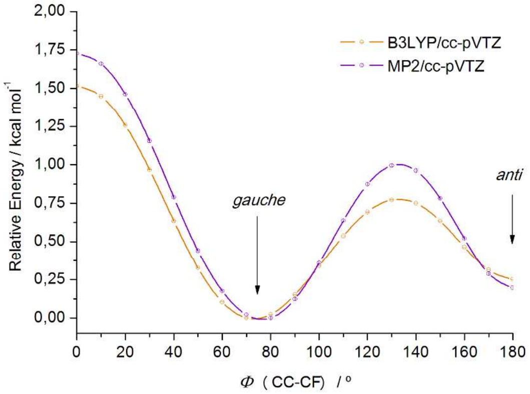

Figure 1. Potential energy curve for PFPF with respect to the Φ(C4C3−C2F1) dihedral angle.

According to Figure 1, the absolute minimum corresponds to a *gauche*-conformation with a dihedral angle Φ(C4C3−C2F1) of 76.5° (MP2) and 73.1° (B3LYP). At 180° (MP2 and B3LYP) another minimum appears, corresponding to an *anti*-conformation.

These minima were then fully optimized and their harmonic vibrational frequencies were computed using the same levels of theory (Figure 2). The difference of the calculated thermal energies (ΔE/kcal mol^{-1}) and Gibbs free energies (ΔG/kcal mol^{-1}) of the second conformation (*anti*) against the *gauche*-conformer are detailed in Table 1. The populations (χ) of each conformation were estimated by using the Boltzmann distribution at 298 K considering that the *gauche*-conformer is doubly degenerated by symmetry considerations.

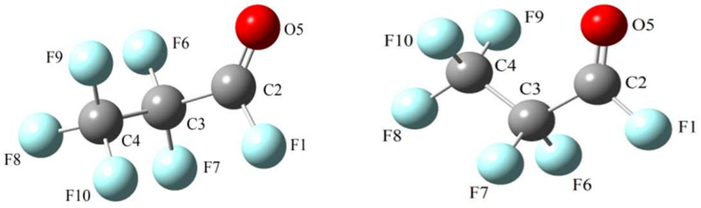

Figure 2. Optimized conformations of *gauche* (left) and *anti* (right) PFPF.

Table 1. Calculated *anti–gauche* thermal energy difference ΔE and Gibbs free energy ΔG. The fraction of population χ for each conformer was calculated at 298 K

	MP2/cc-pVTZ	B3LYP/cc-pVTZ
ΔE(kcal mol^{-1})	0.23	0.28
ΔG(kcal mol^{-1})	0.49	0.46
χ(*anti*) (%)	18.0	18.6

The used approximations reproduced the *gauche*-form as the most stable conformer. This is remarkable, especially taking into account that for 3,3,3-trifluoropropionyl fluoride, $CF_3CH_2C(O)F$, the *anti*-conformation has been reported to be the most stable form.[27] In order to rationalize this singular behavior quantum-chemical calculations at the B3LYP/6-31G level of approximation have been also performed for both $CF_3CF_2C(O)F$ (PFPF) and $CF_3CH_2C(O)F$ computing the results obtained by removal of electron delocalization, i.e., by deleting all non-localized NBOs (anti bonding molecular orbitals) from the basis set in the NBO calculations. The full, localized (L), and non-localized (NL) electronic energetic contribution differences (*anti*-*gauche*) are listed in Table 2 for these compounds. The data show that the delocalized contributions are more important than the localized ones for PFPF. This can be understood in terms of a stabilization of the *gauche*-conformation due to electron delocalization from the bonding to the antibonding molecular orbitals. For $CF_3CH_2C(O)F$, although the

NL contribution favors the *gauche*-conformer, the localized factor exceeds the delocalized contribution, stabilizing the *anti*-conformation.

Table 2. *Anti-gauche* full localized (L) and delocalized (NL) energy contribution differences for both $CF_3CF_2C(O)F$ and $CF_3CH_2C(O)F$ molecules (kcal mol^{-1})

	$CF_3CF_2C(O)F$	$CF_3CH_2C(O)F$
ΔE(full)	0.48	–1.03
ΔE(L)	–4.02	–0.59
ΔE(NL)	4.50	0.44
ΔE(NL)+ΔE(L)	0.48	–0.15

As can be seen from the Figure 2, the bonds C3−F6 and C3−F7 are oriented in a different way with respect to both the C2=O5 and C2−F1 groups in both the most stable *gauche* and *anti*-conformations. In the *anti-conformation* both C3−F6 and C3−F7 bonds are in different planes from the C2=O5 and C2−F1 groups, while in the *gauche*-conformer C3−F6 and C3−F7 are almost coplanar with the C2=O5 and C2−F1 groups, respectively. This relative arrangement causes the stabilization of the *gauche*- over the *anti*-conformation. Thus, a stabilizing interaction between the π(C2=O5) and the σ*(C3−F6) molecular orbital is only allowed in the *gauche*-conformation.

In order to quantify these electron delocalization energies in the PFPF molecule, quantum-chemical calculations (B3LYP/6-311+G(d)) have been performed where specific donor-acceptor interactions were removed. The energy of a concrete donor-acceptor interaction was computed by the subtraction of the energy obtained with specific removed interactions from the full electronic energy. These energies are listed in Table 3. As can be seen from this table, the contribution from the π(C2=O5)→σ*(C3−F6) interaction for the *gauche* form is one order of magnitude higher than the rest of the interactions and responsible for the stabilization of the *gauche*- over the *anti*-conformation.

Table 3. Specific electron delocalization energies of PFPF

Molecular Orbitals		ΔE (kcal mol^{-1})	
Donor	Acceptor	*gauche*	*anti*
σ(C2−F1)	σ*(C3−F6)	–0.061	–0.067
σ(C2−F1)	σ*(C3−F7)	–0.049	–0.047

π(C2=O5)	σ*(C3−F6)	–0.302	–0.068
π(C2=O5)	σ*(C3−F7)	0	0

UV/vis spectrum

The experimental gas UV/vis spectrum of PFPF presents only one maximum located at 214.0 nm. Quantum-chemical calculations (TD − B3LYP/6-311+G(d)) reproduce the maxima at 222 and 221 nm fairly well for the *anti*- and *gauche*-conformers, respectively. According to these calculations, the transition σ(C=O)→π*(C=O) causes these bands. Moreover, another transition (LP(O)→π*(C=O)) occurs simultaneously at 221 nm for the *gauche*-conformer. In the case of the *anti*-form the former transition takes place at 165 nm. Figure 3 compares the experimental and computed gas UV/vis spectrum for PFPF.

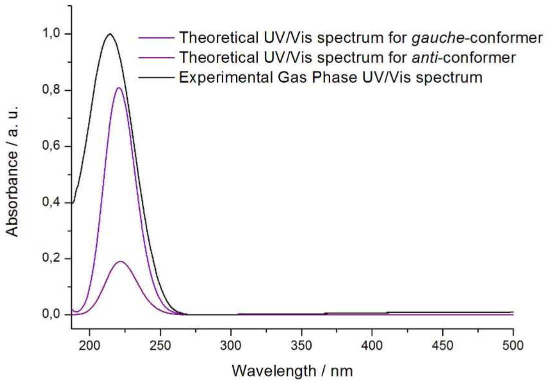

Figure 3. Gas and computed (TD − B3LYP/6-311+G(d)) UV/vis spectra for PFPF. The theoretical spectrum was calculated using a composition of 81 % *gauche* and 19 % *anti*.

Infrared spectrum

The optimized structures of both *gauche*- and *anti*-conformations were used to calculate the IR harmonic frequencies. These frequencies were corrected by the reported scale factors: 0.949 (MP2/cc-pVTZ) and 0.965 (B3LYP/cc-pVTZ).[28] The computed spectra calculated for a mixture of both conformations show a very good agreement with the experimental one (Figure S3). This comparison allowed us proposing an assignment of all normal modes of vibration. Figure 4 illustrates the experimental gas FTIR and its comparison with the computed spectra for both *anti*- and *gauche*-

conformers. These Figures, in particular Figure 4 b, show only few features – the broadening of the bands at 1345, 1236 and 1013 cm^{-1} – that possibly indicate of the presence of an *anti*-conformer.

The strongest IR band located at 1132 cm^{-1} can be assigned with confidence to the C−F stretching vibration mode due to its characteristic intensity and location.[29,30] On the other hand, the second most intense band in this spectrum corresponds to the carbonyl stretching normal mode of vibration (1889 cm^{-1}). A complete assignment of the infrared spectrum is presented in Table S6.

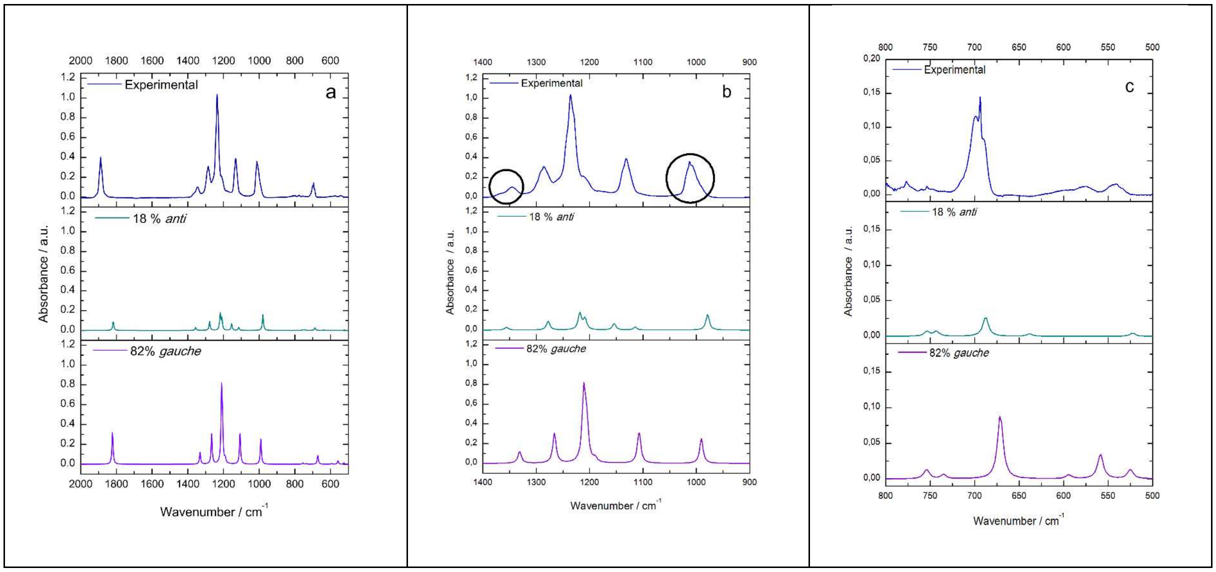

Figure 4. Gas FTIR spectrum of PFPF (top) and computed IR spectra for the *anti*-conformer (middle) and *gauche*-conformer (down). The relative computed weighted composition of these two forms is taken into account in the absorbances: complete spectra (a), sections between 1400 and 900 cm^{-1} (b) and between 800 and 500 cm^{-1} (c).

The signal at 694 cm^{-1} in the gas FTIR spectrum of PFPF presents a defined “A” band contour (see Figure 4 c). The oscillation of the FCO scissor-deformation vibration of the most abundant conformer with respect to the A principal axis of inertia gives rise to this band with the corresponding contour (Figure S4).

Matrix isolated $CF_3CF_2C(O)F$ in Ar (1:300)

A gas mixture of PFPF in Ar (1:300) was trapped onto a CsI window at a temperature of ca. 15 K and the FTIR spectrum of this solidified mixture was obtained (Figure 5). The band assignments of both *anti*- and *gauche*-conformers could be straightforwardly performed from the FTIR matrix-isolation spectrum shown in Figure 5 where the small population of the *anti*-conformer is clearly observed.

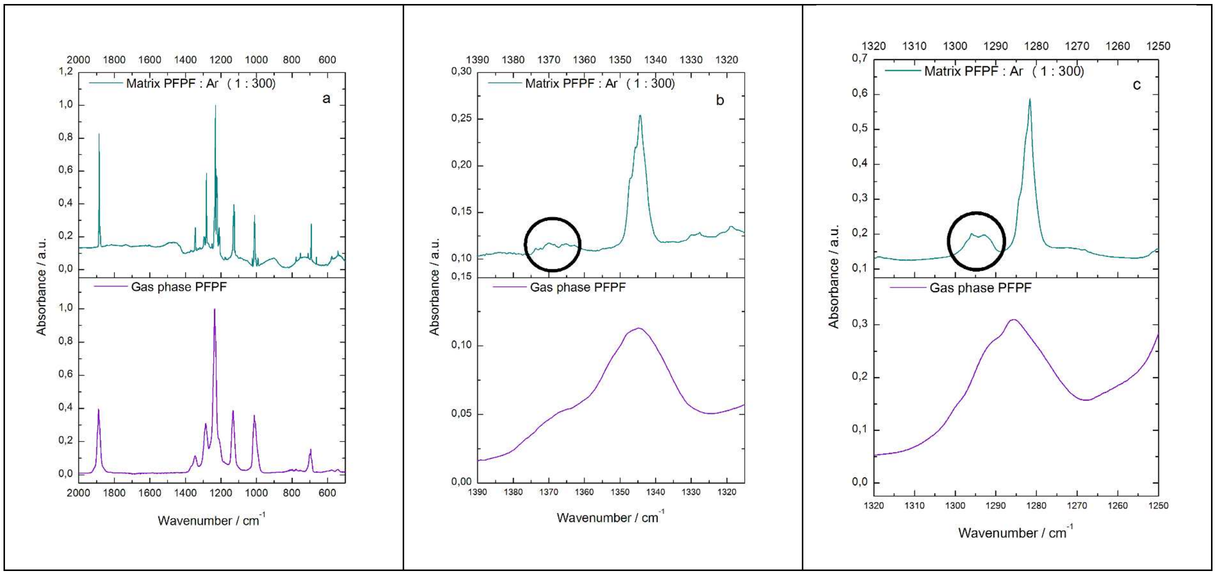

Figure 5. Gas and Ar-matrix (1:300) FTIR of PFPF. Complete spectra (a) and 1390 – 1325 cm^{-1} (b) and 1320 – 1250 cm^{-1} regions (c). Black circles indicate the contribution of the *anti*-PFPF conformer.

Annealing

After performing one annealing step of 10 K the concentrations of the *anti*- and the most populated *gauche*-conformers were found to be smaller, while simultaneously the formation of a dimer species is observed.

Structural study of dimeric PFPF

In order to obtain the dimeric structure, the length of the RO···C(O)R intermolecular interaction obtained from XRD data (see XRD section below) was first optimized in an energy curve at B3LYP/6-311+G(d) level of approximation. The minimum was subsequently optimized using the same theoretical method and its harmonic vibrational frequencies were then computed. The structure corresponds to a double-*gauche* dimer with a O···C=O length and angle of 3.04 Å and 90.3°, respectively (see Figure 6).

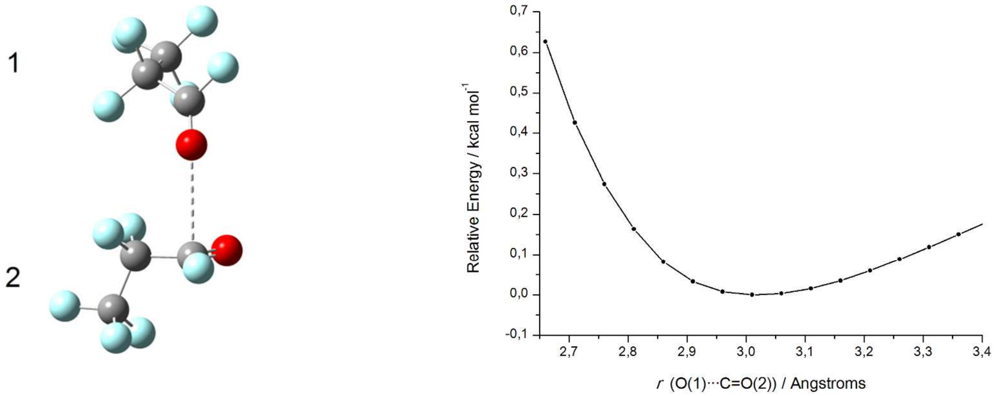

Figure 6. Left: Quantum-chemically optimized dimer of PFPF. Right: Relative energy of the PFPF dimer (kcal mol^{-1}) with respect to the O(1)···C=O(2) length.

The small contribution of the *anti*-conformer under these experimental conditions precludes further analysis related to this species. FTIR spectra of the diluted PFPF in Ar at cryogenic temperatures before and after an annealing of 25 K are depicted in Figure 7. The corresponding assignment was performed with the assistance of computed values. Table S6 shows the assignment of all bands observed in the matrix spectra.

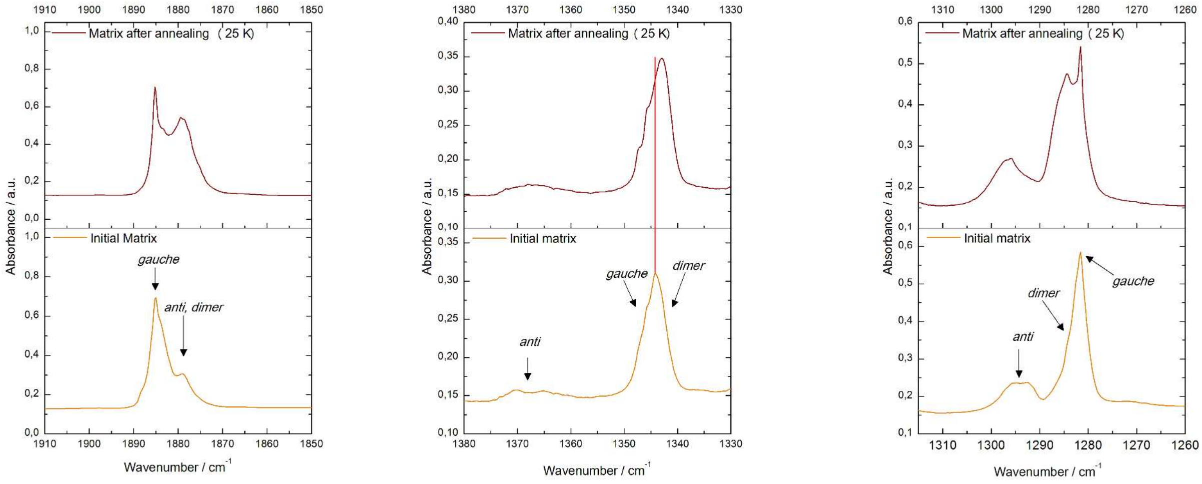

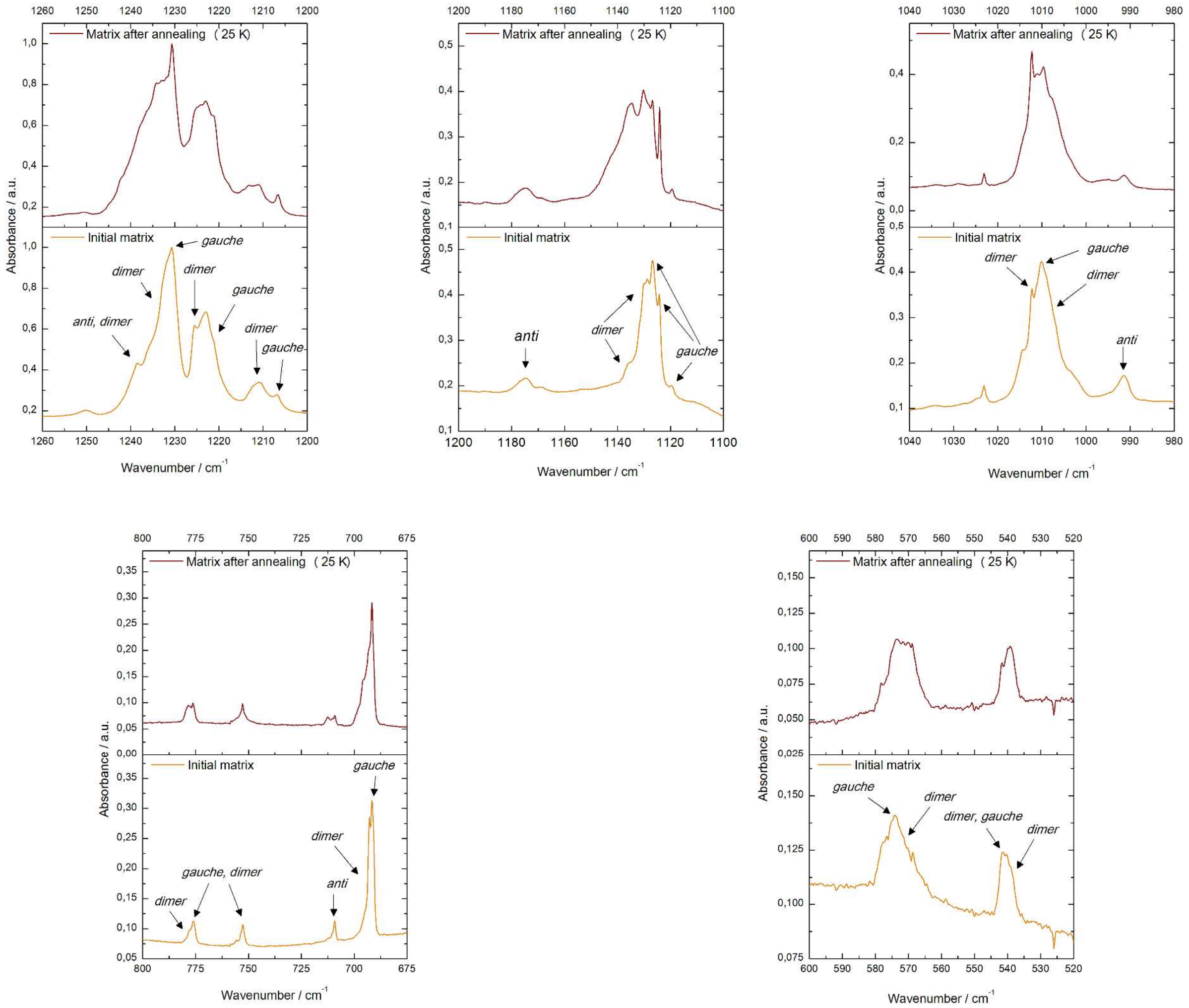

Figure 7. Comparison of the matrix FTIR spectra of PFPF diluted in Ar 1:300 before (15 K) and after annealing at 25 K.

Matrix isolated $CF_3CF_2C(O)F$ in Ar (1:1000)

UV-Vis broad band irradiation

A sample of PFPF diluted 1:1000 with argon at cryogenic temperatures was exposed to UV-vis broad band irradiation ($200 \leq \lambda \leq 800$ nm). FTIR spectra were taken at different irradiation times (t), i.e. without irradiation and at 0.25, 1, 4, 8, 16, 32 and 64 min. The effect of the irradiation is to originate the rupture of the dimer structures linked by van der Waals forces with a subsequent increase in the concentration of the monomeric units. The evolution of the relative areas of selected bands belonging to both, dimer and *gauche*-species, is shown in Figure 8. No further photoevolution was observed in the matrix.

The situation is completely different when PFPF is irradiated in the gaseous state. Cariati *et al*. reported that PFPF irradiated in the 232 − 240 nm region undergoes a photoevolution generating CO, C_4F_{10} and COF_2 according to Scheme 1.[31] This process is not allowed in matrix conditions since it needs the coincidence of two molecules of monomeric PFPF.

Scheme 1: Reported photochemical evolution of gaseous PFPF.

$$2\ CF_3CF_2C(O)F + h\upsilon \rightarrow CO + C_4F_{10} + OCF_2$$

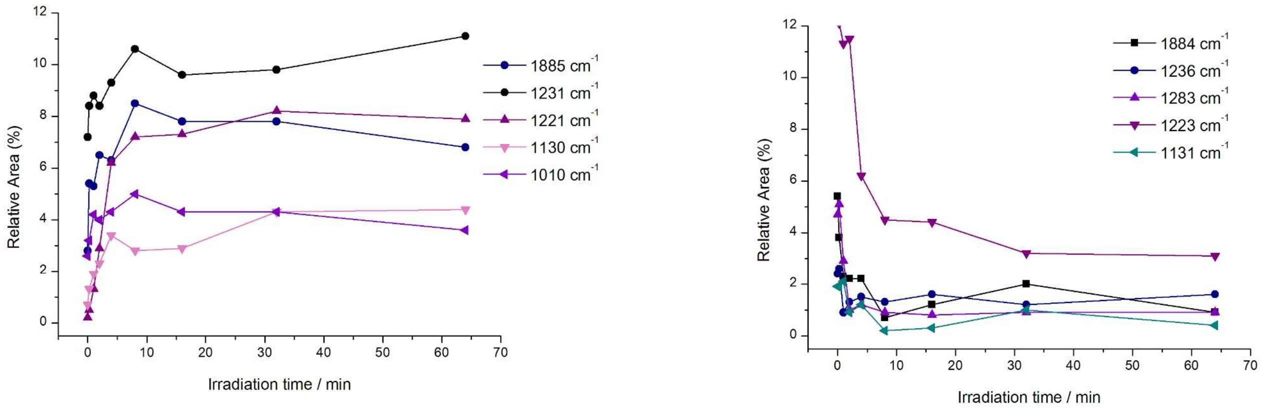

Figure 8. Relative areas (%) of selected FTIR bands of the dilution of PFPF in Ar (1:1000) at cryogenic temperatures. On the left and right side of the figure the photoevolution of bands corresponding to the g*auche*-conformers and the dimer are shown, respectively.

Annealing after photolysis

The FTIR spectra of the diluted PFPF in Ar (1:1000) at cryogenic temperatures taken before and after an annealing at 25 K are depicted in Figure 9. The assignment was again performed with the assistance of computed values. Table S6 lists the assignment of all bands found in the matrix spectrum. This diluted matrix shows a relative diminution of the dimer species in comparison with the conformational equilibrium of the free forms.

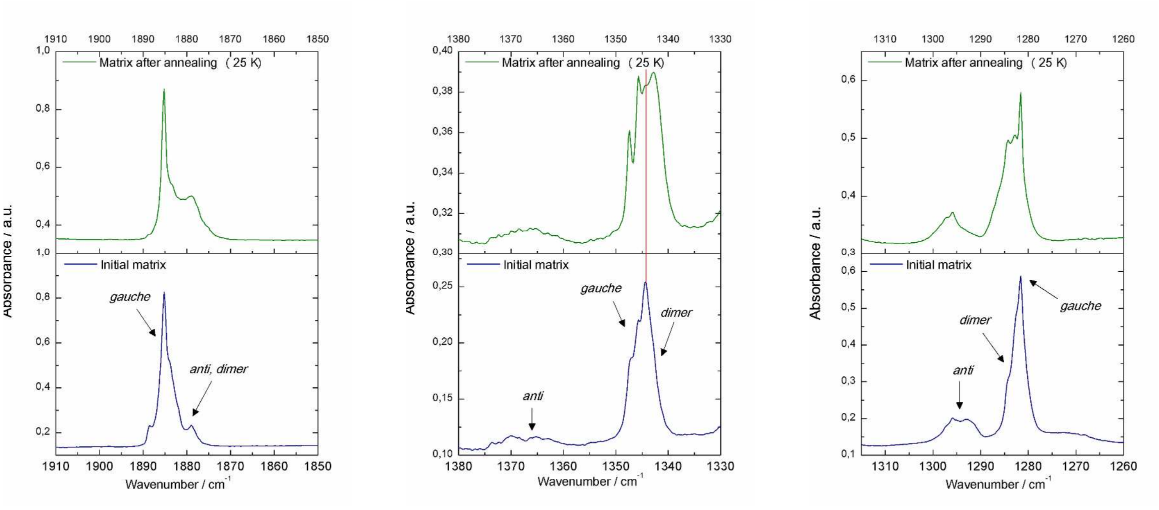

Figure 9. Different sections of Ar-matrix (1:1000) FTIR spectra of PFPF before and after annealing. a) Between 1910 and 1850 cm^{-1}, b) between 1380 and 1330 cm^{-1} and c) between 1315 and 1260 cm^{-1}.

The diffusion of the species near the boiling point of the Ar allows the regeneration of the dimer even at higher concentrations than the originally deposited from the mixture at room temperature.

Liquid phase Raman spectrum

Figure 10 presents the comparison between the liquid phase Raman spectrum of PFPF and its computed spectrum (MP2/cc-pVTZ) of a 18 % *anti* and 82 % *gauche* weighted conformer composition. This figure provides another clear evidence of the contribution of the *anti*-rotamer through the band at 329 cm^{-1} in agreement with the proposed assignment on Table S6.

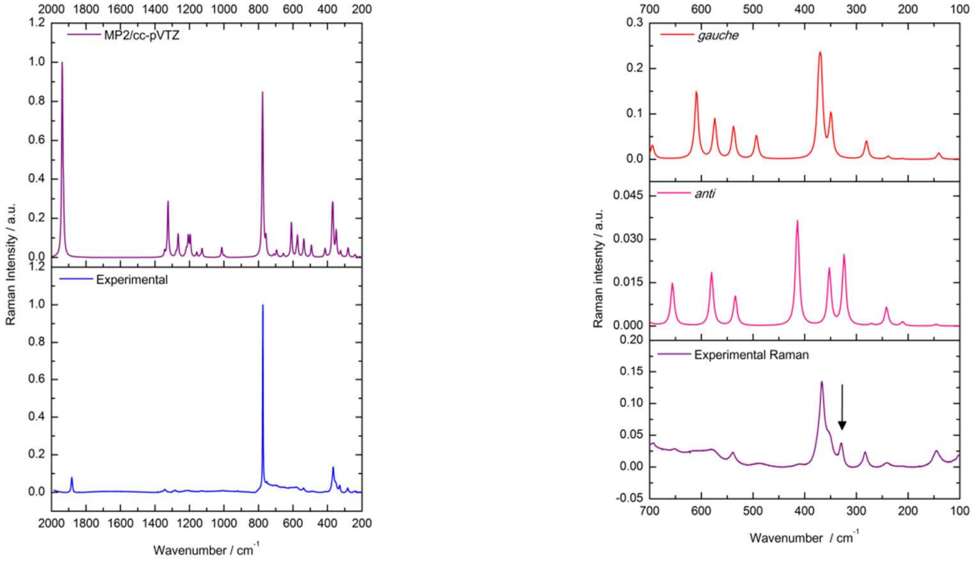

Figure 10. Left: Comparison between the liquid Raman spectrum of PFPF and the computed (MP2/cc-PVTZ) spectrum. Right: Comparison between the computed spectra for the *anti*- and *gauche*-conformers in the region between 700 and 100 cm^{-1} with the experimental liquid phase Raman spectrum. The arrow in the experimental spectrum indicates the contributions of the *anti*-rotamer.

Gas Phase Structure

Electron scattering intensities for gaseous PFPF have been recorded using the electron diffractometer at Bielefeld University. Computed geometries (MP2/cc-pVTZ) of the two stable conformations, *gauche* and *anti* were used as starting geometries for the least-square refinements of the structural parameters of PFPF by GED. The radial distribution functions are presented in Figure 11. The quality of fit of the two-conformer model can be assessed by the flatness of the difference curve and by the final *R*-factor of 4.65 %. The GED experiment reveals a conformational composition of 85(10) % *gauche* and 15(10) % *anti* (three times standard deviations are in parentheses). According to the Hamilton criterion[32] the relative amount of anti-conformer is in the range between 10 and 20% at a significance level of 99% (a plot is provided in the supplementary information: Figure S5). The previously described calculations are qualitatively consistent with the GED experiment. Relevant geometric parameters obtained by XRD, GED and theoretical calculations are listed and compared in Table 4. The refined in GED Cartesian coordinates of both *gauche*- and *anti*-conformers are listed in Tables S8 and S9, respectively. Refined interatomic distances and vibrational amplitudes are presented in Tables S4 and S5, respectively.

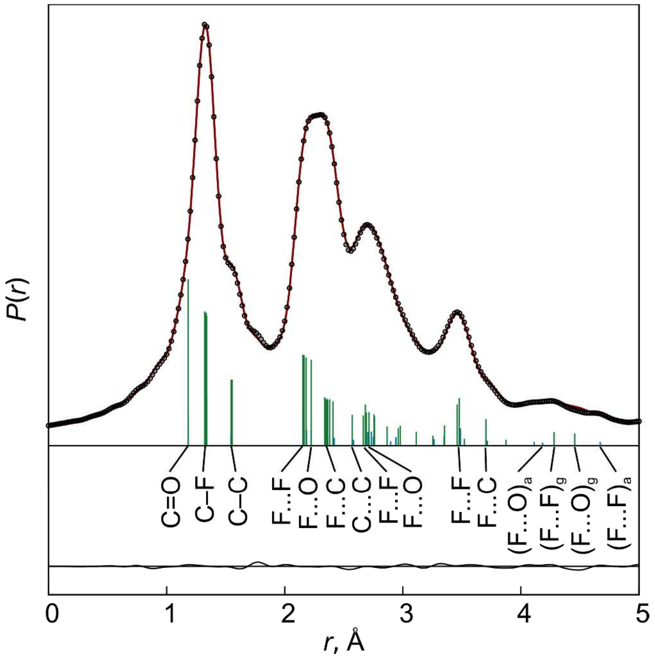

Figure 11. Experimental (dots) and model (continuous line) radial distribution functions for PFPF. Vertical lines correspond to interatomic distances in both conformers; most important are assigned here; for the exact numeration and the full list of terms see Tables S4 and S5.

Crystal Structure

The crystal structure of PFPF (Figure 12) contains only molecules in the *gauche*-conformation. Their structure resembles that described for the most stable form in the gas phase.

Crystals of PFPF belong to the space group *Pbca* (no. 61) with metrics a = 9.0597(7) Å, b = 6.1421(5) Å, c = 18.7284(13) Å. V = 1042.16(13) Å^3, Z = 8, μ(Mo-Kα) = 0.289, 28654 reflections measured, 1028 unique (Rint = 0.0390) which were used in all calculations. The final wR_2 was 0.1014 for all data and R_1 was 0.0390 for 994 reflections with $I > 3\sigma(I)$. Structural parameters are shown in Table 4. All crystallographic data obtained from the structural analysis and refinement of PFPF are provided in Table S7.[33]

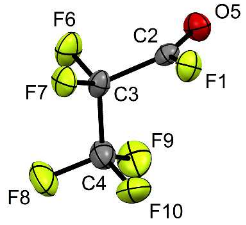

Figure 12. PFPF crystal structure (*gauche*-conformation).

In general, the structural parameters obtained with the different methods are comparable. As expected in view of the different phases involved, values of the dihedral angles present a noticeable dependence on the technique, especially those regarding to the *gauche*-conformation, where differences are found for the solid and gas structure. This can be explained in terms of the intermolecular interactions present in the solid.

Table 4. Experimental GED, XRD and theoretical structural parameters of *gauche*, and *anti*-PFPF[a]

Parameter	*gauche*					*anti*			
	GED		XRD	MP2	B3LYP	GED		MP2	B3LYP
	r_g	r_e, $\angle_e$	r_α, $\angle_\alpha$	r_e, $\angle_e$	r_e, $\angle_e$	r_g	r_e, $\angle_e$	r_e, $\angle_e$	r_e, $\angle_e$
C=O	1.183(5)	1.178(5)	1.166(2)	1.183	1.175	1.184(5)	1.180(5)	1.185	1.176
C(O)-F	1.332(1)	1.324(1)	1.324(2)	1.333	1.338	1.332(1)	1.325(1)	1.333	1.338
$(C\text{-}F)_{av}$	1.331(1)	1.324(1)	1.328(3)	1.333	1.339	1.332(1)	1.325(1)	1.334	1.340
C(O)-C	1.548(3)	1.536(3)	1.535(3)	1.536	1.546	1.546(3)	1.533(3)	1.533	1.542
C-C	1.556(3)	1.542(3)	1.531(3)	1.542	1.555	1.553(3)	1.540(3)	1.539	1.552
C(O)-C-C		112.4(9)	111.8(2)	112.4	113.2		113.2(9)	113.2	113.7
F-C=O		124.9(8)	123.1(2)	124.0	123.8		124.7(8)	123.8	123.5
C-C=O		124.0(21)	125.8(2)	125.9	126.1		125.4(21)	127.3	127.4
C-C(O)-F		111.1(22)	111.1(2)	110.0	110.1		110.0(22)	108.9	109.1
$(C\text{-}C\text{-}F)_{av}$		109.1(1)	109.7(2)	109.2	109.2		109.1(1)	109.1	109.1
$(F\text{-}C\text{-}F)_{av}$		109.3(4)	108.9(2)	109.2	109.0		109.2(4)	109.1	109.0
F-C(O)-C-C		76.2(62)	86.8(2)	75.6	73.1		180.0[b]	180.0	180.0

[a] Bond length are Å, angles in degrees. In parentheses are three times standard deviations obtained from least squares analysis. See Supporting Information for details about refinement of structures in GED. MP2 and B3LYP calculations were done with cc-pVTZ basis set to compute both the analytical harmonic and the numeric cubic force fields.

[b] Assumed parameter.

Intermolecular assembly in solid state

Six intermolecular contacts with lengths shorter than the sum of the van der Waals radii (vdW) of the involved atoms were detected from the XRD experimental data. All of them are listed in Table 5 along with their corresponding length, the difference between their length and the sum of the involved van der Waals radii, r_{vdW}.[34]

Table 5. List of intermolecular contacts

Atoms involved	Length	Length−r_{vdW}[a]
O5···C2[a]	2.803(2)	–0.417
F8···F6[b]	2.848(2)	–0.092
F7···F9[c]	2.886(2)	–0.054
O5···C3[a]	3.171(3)	–0.049
F1···C2[d]	3.129(2)	–0.041
O5···F7[a]	2.970(2)	–0.020

a 3/2–*X*,-1/2+*Y*,+*Z*; b 1/2+*X*,1/2–*Y*,1–*Z*; c +*X*,–1+*Y*,+*Z*; d 2–*X*,–1/2+*Y*,3/2–*Z*

The second-order perturbation stabilization energy *E*(2) which relates the charge transfer within donor and acceptor orbitals were computed for adjacent molecules at the NBO B3LYP/6-311+G(d) level of approximation. In order to perform this calculation a system centered in one molecule coordinated by eight molecules as in the crystal phase was used.[35]

Table 6 lists these interactions together with the second order perturbation energy (ΔE^2) and the donor/acceptor character of the corresponding orbitals that participate in these contacts among other parameters.

Table 6. List of intermolecular contacts in the crystal structure of PFPF. The direction of the arrow is defined by the donor/acceptor character of the orbital involved

Atoms involved			ΔE^2/kcal mol^{-1}	Donor orbital	Acceptor orbital
O5	→	C2	0.88	LP(1)O	π*(O=C)
F8	↔	F6	0.15	LP(1)F8/6	RY*F6/8
F7	→	F9	0.08	LP(3)F	RY*F
O5	→	C3	0.05	LP(2)O	σ*(C3−C4)
F1	→	C2	0.07	LP(3)F	π*(O=C)

O···C interactions

Two different O···C interactions were reported from the XRD analysis of PFPF crystal structure. The NBO analysis demonstrates a high contribution of electron delocalization between one oxygen lone pair (LP) and the π*(O5=C2) molecular orbitals, and between the second oxygen lone pair and the antibonding σ*(C3−C4) molecular orbital. The second order perturbation energies (ΔE^2) involved in both cases are 0.88 and 0.05 kcal mol^{-1}, respectively.

This O···C=O intermolecular interaction is the basis for the dimer formation of the substance evidenced in the matrix experiment and can be further described in terms of geometric parameters. For PFPF the perpendicular interaction within the carbonyl groups is preferred over the parallel, where the C···O=C angle is 163.3(2)°, a value that perfectly fits in the 150−180° range found in the literature for these orthogonal interactions.[36] Defining a mean plane by C3, O5 and F1 the vector pointing from O5 of the neighbor molecule to C2 shows a nearly perpendicular angle of 83.7(1)° to this plane (Figure 13). In addition, the PFPF carbonyl carbon C2 gets 0.013(2) Å out of this plane due to its interaction with the nucleophilic oxygen atom O5 from the neighbor molecule.

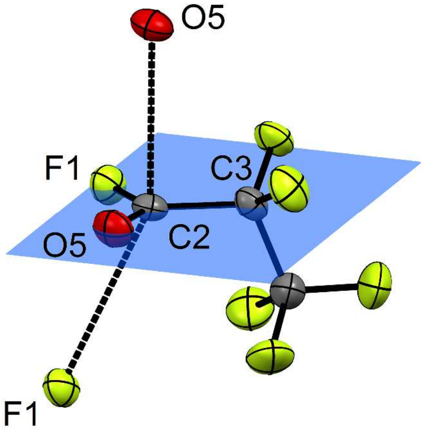

Figure 13. Plane formed by F1–C3 and O5.

C–F···F–C interactions

Attractive F···F interactions have been the subject of controversial discussions. In 1989 Desiraju *et al.*[37] questioned their nature in terms of halogen···halogen interactions, concluding that no stabilization was generated by them in close packing. Later on, Bianchi, Forni and Pilati, determined an experimental charge density demonstrating that F···F intermolecular interactions clearly contribute to the stabilization of crystal packing in the donor acceptor complex of (E)-1,2-bis(4-pyridyl)ethylene with 1,4-diiodotetrafluorobenzene.[38] Furthermore, Matta *et al.* proved that some intramolecular F···F contacts present in crystals of aromatic compounds behave as weak closed-shell interactions with stabilization energies up to 14 kcal mol^{-1}.[39] Intramolecular F···F contacts were also described in a charge density study of 2,3,5,6-tetrafluoro- and pentafluoro-pyridine; in both molecules there are weak F···F and F···C type interactions, but they become less important for determining the intermolecular arrangement, when the stronger F···H type interactions are also present, like in 2,3,5,6-tetrafluoro-pyridine.[40] A remarkable fact about F···F interactions became evident in the crystal structure of haloperidol, an antipsychotic drug, where these interactions are preferred over the more common Cl···Cl halogen contacts.[6] Chopra and coworkers have recently expressed that, despite the fact that there is evidence for many F···F intermolecular interactions, the exact nature of these interactions remains still unclear.[1]

In the present case of PFPF, two F···F contacts have been detected in its crystal structure. According to Reichenbächer[2] a total of 788 compounds with F···F distances below 3 Å could be found in the Cambridge Structural Database (CSD),[41] by the year 2005. As can be seen from Table 5 and Figure 14, both F···F lengths present in the PFPF crystal resemble the reported values. An angle analysis of these intermolecular interactions allows complementing the structural characterization. In this regard, Desiraju *et al*.[37] classified halogen interactions into type I when $\theta_1 \approx \theta_2$ and type II if $\theta_1 \approx 180°$ and $\theta_2 \approx 90°$, where θ are the angles involving the F···F interaction. Table 7 presents these interactions in conjunction with the respective angles values (Figure 14) and allows the conclusion that both F···F interactions in solid PFPF belong to type I.

Table 7. θ_1 and θ_2 values of PFPF inter-fluorine intermolecular contacts

Involved atoms	Angle			Interaction type
F6···F8	C3−F6···F8	θ_1	167.2(1)°	I
	F6···F8−C4	θ_2	138.2(1)°	
F7···F9	C3−F7···F9	θ_1	157.5(1)°	I
	F7···F9−C4	θ_2	155.3(1)°	

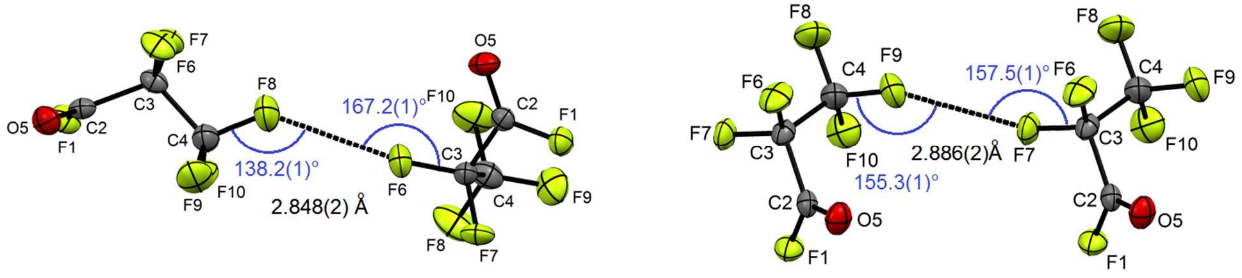

Figure 14. Schemes of F6···F8 (left) and F7···F9 (right) intermolecular interactions.

In most cases, type I interactions involve a crystallographic inversion center. The type I CF···FC interaction in PFPF is an exception to this generalization since the involved fluorine atoms are not equivalent. The stabilizing delocalization energy obtained by NBO calculations (see Table 6), corroborates that both fluorine atoms (F6 and F8) involved in a F···F interaction act as electron donor and acceptor at the same time, being a lone pair orbital and a Rydberg orbital the donor and the acceptor orbitals, respectively. On the other hand, F7 and F9 participate in a polarized F···F contact, being F7 an electron donor to F9 an electron acceptor.

C−F···C=O interactions

The contact between the fluorine and carbon atoms is, according to the NBO analysis, caused by the electron delocalization from one fluorine lone pair and the π-carbonyl antibonding molecular orbital (C−F···C=O). The first study of intermolecular interactions involving organic fluorine and carbonyl groups has been reported by Olsen and co-workers.[42] They performed an exhaustive search of the Cambridge Structural Database (CSD),[33] finding 43 close C−F···C=O contacts shorter than the sum of the C and F van der Waals radii out of a total of 573 interactions of this kind. According to these statistics ran over the 573 contacts, the intermolecular C−F···C=O length (d_1) covers a range from 2.5 to 4.0 Å, a C···F−C angle (α_1) a range between 100 and 160º and the fluorine atom involved in the mentioned intermolecular contact tends to be in a position nearby the pseudotrigonal axis of the C=O unit. Our results for PFPF are included in the precedent reported ranges (see Figure 15).

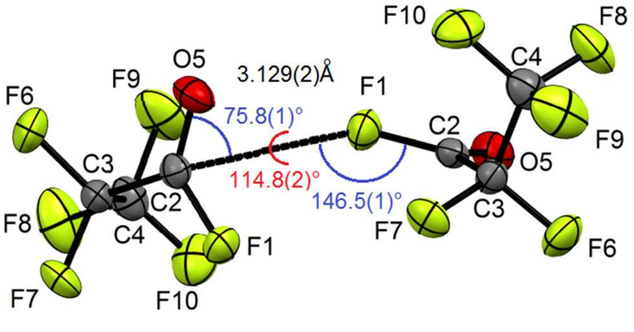

Figure 15. C−F···C=O intermolecular contact between two PFPF molecules. The bond length d_1(C−F···C=O) = 3.129(2) Å, the dihedral angle Φ(C−F···C=O) = 114.8(2)º, the angles α_1(C···F−C) = 146.5(1)º and α_2(O=C···F) = 75.8(1)º are highlighted

O···F interactions

According to the XRD data (Table 5), the O···F interaction appears to be negligible when it is compared with the previously described types of contact. Moreover, such interactions do not seem to be relevant in the NBO calculation, that's why they are not listed in Table 6.

In 1983 Murray-Rust *et al*. studied the crystallographic environment of different fluorinated carboxylic acids, dividing the intermolecular interactions involving C−F groups into three categories.[43] The second of those categories, C−F···O and C−F···N, is of particular interest in this section. The PFPF C−F···O intermolecular contact (2.97 Å) fits in the 2.85 Å < *d* (C−F···O) < 3.2 Å interval found by running a statistics over 71 C−F···O interactions.

Conclusion

We prepared and characterized perfluoropropanoyl fluoride (PFPF) using vibrational spectroscopy in different phases. The assignment of the vibrational normal modes was based on quantum-chemical calculations.[44] Matrix isolation coupled to IR spectroscopy allowed resolving the contributions of the *anti*- and *gauche*-conformations, and in addition of a dimeric species formed by *gauche*-rotamers. The effect of increasing the concentration of PFPF under matrix conditions results in an increased concentration of dimer, while heating up to 10 ºC (by means of an annealing) induced cleavage of the dimers into *gauche*-monomers.

The structure of the title compound has been also explored in both, crystal and gas phase, by XRD and GED, respectively. The crystal structure manifests different types of intermolecular interactions; they were analyzed in terms of geometry and type and strength of overlap by supporting NBO calculations. The structure of $CF_3F_2C(O)F$ in the gas phase allowed studying the geometry without any intermolecular distortions; the conclusion is that the intermolecular interactions in the crystal are too weak to cause substantial distortion of the molecular structure in this case.

While the *gauche*-conformation is the sole form present in the crystalline state, the GED data indicate that both conformations, *gauche* and *anti*, are present in equilibrium in the gaseous phase. This is reproduced by quantum-chemical calculations for single molecules. The *gauche*-conformer represents the absolute minimum in energy, and due to symmetry degeneration, is far more abundant in the gas. This is not the case reported for the less fluorinated $CF_3CH_2C(O)F$ for which the *anti*- was determined to be more stable than the *gauche*-conformer.[27] As a result, a comparison of these two compounds and their possible conformations was undertaken. NBO calculations indicate that in the case of $CF_3CH_2C(O)F$ steric effects predominate, that stabilize the *anti*-conformer, but in $CF_3CF_2C(O)F$ with dominating *gauche*-conformation, delocalization effects, especially the interaction $\pi(C2=O5)\rightarrow\sigma^*(C3–F6)$, are more important.

ACKNOWLEDGEMENT

The authors thank Deutsche Forschungsgemeinschaft (scholarship for Y. B. M. in Germany and core facility GED@BI), Alexander von Humoldt Siftung (stipend for Yu. V. V.), Agencia Nacional de Promoción Científica y Técnica (ANPCyT), Consejo Nacional de Investigaciones Científicas y Técnicas (CONICET), Comisión de Investigaciones de la Provincia de Buenos Aires (CIC), Facultad de Ciencias Exactas, Universidad Nacional de La Plata (UNLP) and Bielefeld University for financial support.

Supporting information available:

Total intensity curves and additive background lines of PFPF for short and long nozzle-to-plate distances (Figure S1), experimental and model molecular intensity curves of PFPF for short and long nozzle-to-plate distances (Figure S2), experimental and theoretical B3LYP/cc-pVTZ and MP2/cc-pVTZ IR spectra of PFPF (Figure S3), principal axes of inertia of *gauche*-PFPF and the derivative dipole unit vector corresponding to the δ_{sciss}(COF) vibrational normal mode (Figure S4) and dependence of the GED total R-factor on the relative amount of anti conformer (Figure S5). Set up of the GED experiments (Table S1), Z-matrices (Tables S2–S3), best interatomic distances, mean square amplitudes and vibrational corrections (Tables S4–S5), comparison between experimental and theoretical vibrational bands corrected with the corresponding scale factors and the corresponding proposed assignment (Table S6), crystallographic data (Table S7), refined Cartesian coordinates of *gauche* and *anti*-$CF_3CF_2C(O)F$ in GED (Table S8 and S9).

References

---

1 Chopra, D.; Guru Row, T. N. Role of organic fluorine in crystal engineering. *CrystEngComm*. **2011**, *13*, 2175–2186.

2 Reichenbächer, K.; Süss, H. I.; Hulliger, J. Fluorine in crystal engineering- "the little atom that could". *Chem. Soc. Rev*. **2005**, *34*, 22–30.

3 Bhhatarai, B.; Gramatica, P. Per-and Polyfluoro Toxicity (LC50 Inhalation) Study in Rat and Mouse Using QSAR Modeling. *Chem. Res. Toxicol*. **2010**, *23*, 528–539.

4 Renner, R. Concerns over common perfluorinated surfactant. *EnvironSci. Technol*. **2003**, *37*, 201A–202A.

5 Mogelberg, T. E.; Sehested, J.; Tyndall, G. S.; Orlando, J. J.; Fracheboud, J.-M.; Wallington, T. J. Atmospheric Chemistry of HFC-236cb: Fate of the Alkoxy Radical CF_3CF_2CFHO. *J. Phys. Chem. A*. **1997**, *101*, 2828–2832.

6 Prasanna, M. D.; Guru Row T. N. Weak interactions involving organic fluorine: analysis of structural motifs in Flunarizine and Haloperidol. *J. Mol. Struct*. **2001**, *562*, 55–61.

7 Vilenchik, Ya. M.; Yakurnova, G. I. Pentafluoroprpionic acid fluoride. *Reak. Osob. Chist. Veshch.* **1979**, *6*, 44–45.

8 Frisch, M. J.; Trucks, G. W.; Schlegel, H. B.; Scuseria, G. E.; Robb, M. A.; Cheeseman, J. R.; Montgomery, Jr., J. A.; Vreven, T.; Kudin, K. N.; Burant, J. C.; Millam, J. M.; Iyengar, S. S. *Gaussian 03*, rev C.02; Gaussian, Inc., Wallingford CT, 2004.

9 Parr, R. G.; Yang, W. Density-Functional Theory of Atoms and Molecules; *Oxford University Press: USA*, **1989**.

10 Møller, C.; Plesset, M. S. Note on an Approximation Treatment for Many-Electron Systems, *Phys. Rev.* **1934**, *46*, 618–622.

11 Gaussian 09 user´s reference. http://www.gaussian.com/g_tech/g_ur/m_basis_sets.htm

12 Foster, J. P; Weinhold F. Natural hybrid orbitals. *J. Am. Chem. Soc*. **1980**, *102*, 7211–7218.

13 E. D. Glendening, J. K. Badenhoop, A. E. Reed, J. E. Carpenter, J. A. Bohmann, C. M. Morales, F. Weinhold, NBO 5.G, Theoretical Chemistry Institute, University of Wisconsin, Madison, WI 2004, http://www.chem.wisc.edu/enbo5/

14 Sipachev, V. A. The use of quantum-mechanical third-order force constants in structural studies. *J. Mol. Struct.* **2004**, *693*, 235–240.

---

15 Sipachev, V. A. Local centrifugal distortions caused by internal motions of molecules. *J. Mol. Struct.* **2001**, *567–568*, 67–72.

16 Sipachev, V. A. Anharmonic Corrections to Structural Experiment Data. *Struct. Chem.* **2000**, *11*, 167–172.

17 Almond, M. J.; Downs, A. J. Spectroscopy of matrix isolated species. *Adv. Spectrosc*. **1989**, *17*, 1–505.

18 I. R. Dunkin. Matrix-Isolation Techniques: A Practical Approach; *Oxford University Press*: New York, **1998**.

19 Perutz, R. N.; Turner, J. J. Pulsed matrix isolation. A comparative study. *J. Chem. Soc., Faraday Trans. 2.* **1973**, *69*, 452–461.

20 Dolomanov, O. V.; Bourhis, L. J.; Gildea, R. J.; Howard, J. A. K.; Puschmann, H. OLEX2: a complete structure solution, refinement and analysis program. *J. Appl. Cryst*. 2009, *42*, 339–341.

21 Sheldrick, G. M. A short history of SHELX. Acta Cryst. 2008, *A64*, 112–122.

22 Berger, R. J. F.; Hoffmann, M.; Hayes, S. A.; Mitzel, N. W. An Improved Gas Electron Diffractometer - The Instrument, Data Collection, Reduction and Structure Refinement Procedures. *Z. Naturforsch*. **2009**, *64b*, 1259–1268.

23 Vishnevskiy, Yu. V. The initial processing of the gas electron diffraction data: An improved method for obtaining intensity curves from diffraction patterns. *J. Mol. Struct.* **2007**, *833*, 30–4.

24 Vishnevskiy, Yu. V. The initial processing of the gas electron diffraction data: New method for simultaneous determination of the sector function and electron wavelength from gas standard data. *J. Mol. Struct.* **2007**, *871*, 24–32.

25 Vishnevskiy, Yu. V. http://unexprog.org, 2015

26 Lynch, B. J.; Truhlar, D. G. How Well Can Hybrid Density Functional Methods Predict Transition Stated Geometries and Barrier Heights? *J. Phys. Chem. A.* **2001**, *105*, 2936–2941.

27 Badawi, H. M.; Förner, W. Vibrational frequencies, normal coordinate analyses and potential functions for internal rotations in 3,3,3-trifluoropropionyl fluoride and 3,3,3-trichloropropionyl chloride based on ab initio calculations. *J. Mol. Struct. (THEOCHEM)*, **1998**, *452*, 85–96.

28 NIST Computational Chemistry Comparison and Benchmark Database, NIST Standard Reference Database Number 101. Release 16a, August 2013, Editor: Russell D. Johnson III http://cccbdb.nist.gov

---

29 Berney, C. V.; Cormier, A. D. Spectroscopy of CF_3COZ compounds- VI. Vibrational spectrum of trifluoroacetyl bromide. *Spect. Acta*. **1977**, *33a*, 929–935.

30 Della Védova, C. O.; Aymonino, P. J.; Bravo, R. D. Spectroscopic Studies on Trifluoroacetyl Iodide, $CF_3C(O)I$. *J. Raman Spectrosc*. **1989**, *20*, 135–140.

31 Cariati, S. A.; Weibel, D. E.; Staricco, E. H. Gas phase photochemistry of perfluoropropyl fluoride and perfluoropropyl chloride. *J. Photochem. Photobio. A: Chem.* **1999**, *123*, 1–5.

32 Hamilton W. C. Significance tests on the crystallographic R factor, Acta Cryst., **1965,** *18,* 502-510.

33 CCDC 1440620 contains supplementary crystallographic data for this paper. These data can be obtained free of charge from The Cambridge Crystallographic Data Centre via www.ccdc.cam.ac.uk/data request/cif

34 Bondi, A. Van der Waals Volumes and Radii. *J. Phys. Chem* **1964**, *68*, 441–452.

35 Berrueta Martínez, Y.; Rodríguez Pirani, L. S.; Erben, M. F.; Reuter, C. G.; Vishnevskiy, Y. V.; Stammler, H. G.; Mitzel, N. W.; Della Védova, C. O. Structure of Chloromethyl Thiocyanate, CH_2ClSCN, in Gas and Crystalline Phases. *Phys. Chem. Chem. Phys*. **2015**, *17*, 15805–15812.

36 Bürgi, H. B.; Dunitz, J. D.; Shefter, E. Chemical Reaction Paths. IV. Aspects of O···C=O Interactions in Crystal. *Acta Crystallogr*. **1974**, *B30*, 1517–1527.

37 Desiraju, G. R.; Parthasarathi, R. The Nature of Halogen···Halogen Interactions: Are Short Halogen Contacts Due to Specific Attractive Forces or Due to Close Packing of Nonspherical Atoms? *J. Am. Chem. Soc.* **1989**, *111*, 8725–8726.

38 Bianchi, R.; Forni, A.; Pilati, The Experimental Electron Density Distribution in the Complex of (*E*)-1,2-Bis(4-pyridyl)ethylene with 1,4-Diiodotetrafluorobenzene at 90 K T. *Chem.-Eur. J.* **2003**, *9*, 1631–1638.

39 Matta, C. F.; Castillo, N.; Boyd, R. J. Characterization of a Closed-Shell Fluorine-Fluorine Bonding Interaction in Aromatic Compounds on the Basis of the Electron Density. *J. Phys. Chem. A*. **2005**, *109*, 3669–3681.

40 Stammler, H. G.; Vishnevskiy, Yu. V.; Sicking, C.; Mitzel, N. W. Charge density studies on 2,3,5,6-tetrafluoro- and pentafluoropyridine. *CrystEngComm.* **2013**, *15*, 3536–3546.

41 Allen, F. H. The Cambridge Structural Database: a quarter of a million crystal structures and rising. *Acta Crystallogr.* **2002**, *B58*, 380–388.

42 Olsen, J. A.; Banner, D. W.; Seiler, P.; Sander, U. O.; D´Arcy, A.; Stihle, M.; Müller, K.; Diederich, F. A Fluorine Scan of Thrombin Inhibitors to Map the Fluorophilicity/Fluorophobicity of an Enzyme Active Site: Evidence for C–F···C=O Interactions. *Angew. Chem*. **2003**, *115*, 2611–2615.

---

43 Murray-Rust, P.; Stallings, W. C.; Monti, C. T.; Preston, R. K.; Glusker, J. P. Intermolecular Interactions of the C–F Bond: The Crystallographic Environment of Fluoriated Carboxylic Acids and Related Structures. *J. Am. Chem. Soc*. **1983**, *105*, 3206–3214.

44 Badawi, H.M.; Forner W. Theoretical Analysis of Two Rotors Internal Rotation and Vibrational Spectra for 2,2,3,3,3-Pentafluororopropionyl Fluoride. *Asian J. Spectr.* **2000,** *4*, 159-171.